Engineering Science and Technology, an International Journal 55 (2024) 101757

Contents lists available at ScienceDirect

Engineering Science and Technology, an International Journal

journal homepage: www.elsevier.com/locate/jestch

Topography simulation of free-form surface ball-end milling through partial discretization of linearised toolpaths

Felipe Marin [a,*], Adriano Fagali de Souza [b], Helton da Silva Gaspar [c], Amaia Calleja-Ochoa [a], Luis Norberto López de Lacalle [a]

[a] Aeronautics Advanced Manufacturing Center (CFAA), University of the Basque Country (EHU/UPV), Bilbao, Spain
[b] Federal University of Santa Catarina (UFSC), Florianópolis, Brazil
[c] Federal University of Santa Catarina (UFSC), Joinville, Brazil

ARTICLE INFO

Keywords:
Free-form
5-axis milling
Ball-end milling
API
CAD
CAM

ABSTRACT

Free-form surfaces are commonly present in several engineering components, from molds to more sophisticated components of aeronautical engines. These parts are usually finished by machining, more specifically, ball-end milling. In this process, the contact between the tool and the part constantly changes along the toolpath, resulting in several manufacturing problems that damage the surface and compromise the performance of the part. Besides the ordinary cutting parameters, these machined surfaces are deeply influenced by the tool tip center and the elastoplastic deformation of the material through the shearing and plowing pair. Knowing the exact orientation of the tool in relation to the surface determines all aspects of the milling process and is necessary for process modeling. The current CAD/CAM software platforms is not able to predict such surface topography. In this direction, the current work presents a software routine developed and implemented on an open interface CAD/CAM software (Siemens® NX). The normal vectors of the surface to be machined, the cutter contact (CC), and cutting location (CL) data from the toolpath calculated by the CAD/CAM were used to obtain a complete discretization of the cutter-workpiece position along the toolpath. This information was used to predict the surface topography and identify the cutting-edge elements. Then, the developed model was used to evaluate the free-form surface of a blade milled on 5-axis together with confocal imaging analysis. The results show that the methodology developed can predict the topography aspects of a free-form machined surface and support the analysis of milling problems such as run-out.

1. Introduction

Free-from surfaces are commonly present in several engineering components, from dies and tools to more sophisticated components of energy and aeronautic industries. During the manufacturing process of such parts, ball-end tooltips are recommended, which can be directly applied on the surface finish or indirectly for manufacturing tools and consumables like electrodes for electrical discharge machining (EDM). Such tools allow different contacts to produce a free-form and smooth surface. However, due to the geometry of the tooltip, it produces crest waves that significantly increase the roughness of the machined surface, which can compromise performance and must be evaluated carefully.

In the design of turbines and aeronautical engines, the shape of the surface of blades, impellers, and blade-integrated disks (BLISKs) can be optimized to improve the aerodynamic flow. This results in complex shape designs, with instantaneous radius changes over the surface that make the manufacturing process challenging. Besides, such parts usually require high strength, wear, and thermal resistance, demanding hard-to-cut materials and increasing design and machining complexities.

The aspect of the surface generated by the milling process significantly impacts the surface integrity and performance, being the most important feature of complex high-performance parts [1]. In blades and aerofoiled components, form errors and other milling process signatures can considerably reduce the component's performance; thus, tight design tolerances are applied to enhance its energetic efficiency. Surface integrity also plays an important aspect in the fatigue life of critical parts, and for this reason, it has been extensively investigated in the last decades [2].

5-axis milling is preferable to finish such parts with free-form geometrical shapes. It allows wider tool access, manufacturing

* Corresponding author.
E-mail address: fmarin004@ikasle.ehu.eus (F. Marin).

https://doi.org/10.1016/j.jestch.2024.101757
Received 1 December 2023; Received in revised form 18 April 2024; Accepted 28 June 2024
Available online 3 July 2024

geometries that would be difficult or impossible to produce with traditional 3-axis due to gouging. Furthermore, it allows modification of the tool's orientation and chip thickness to produce smoother toolpaths, reducing the oscillation of the cutting forces and other related problems [3–5]. Also, it reduces the number of setups, improving lead times and costs.

To guarantee the position of the tool in 5-axis milling, advanced NC controllers are required together with CAM software capable of developing valid and optimized tool trajectories. In this process, the tolerance band must be carefully adjusted to maintain the performance with at least a minimum surface quality. As the tolerance band reduces, more data must be processed, and it can saturate the machine's control loop, resulting in instantaneous reductions or process pauses that severely damage the surface [6]. Also, the data distribution (CL points) inside the tolerance band varies according to the software house, mainly because of different mathematical models used, resulting in different performances for each software in the same machine [7]. Thus, the evaluation of the process commonly considers surface errors and machining time [8].

The topographic aspect of the milled surface using the ball-end tooltip on 5-axis milling can be estimated using different geometrical models that consider the tool position in the space, its diameter, the feed per tooth, the stepover, and the tool run-out. When tool run-out is present, one cusp removes more material, causing different patterns on the surface [9]. The theoretical surface is obtained by computing the engagement between the part and piece, which is an important branch for surface evaluation and prediction. Moreover, geometrical models are required in force prediction, deflection, and form errors. For these reasons, it has been extensively investigated in the last decades [10]. Random surface patterns indicate more complex problems related to vibration, process cinematics, wear, deformations, or clamping issues and must be addressed with the support of other simulation tools. Denkena et al. [11] applied a stochastic method to predict surface topography with high accuracy, considering process imperfections and kinematics. However, it requires prior knowledge of the milling results of a surface machined under such processing conditions, which makes general implementation in software difficult.

Several approaches can be considered to the geometrical model of the cutter. The most common are the analytic model of the helix, the tool dome, and the infinitesimal cutting-edge (ICE) element. The choice between them will depend on the depth and precision required for the analysis. Lazoglu and Liang [12] modelled the engagement and the chip thickness variation during convolution to predict the milling force of ball-end milling on a flat surface. Zhang et al. [13] discretized the tool edge of a ball-end tooltip with a constant helix into a series of cutting points to include the tool wear on the topography surface prediction. Although there is a considerable amount of research on ball-end milling on flat surfaces, its proposed application to milling free-form surfaces still faces several limitations due to the complexities and changes in the CWE.

Ismail Lazoglu [14] solid-modelled the CWE of the 5-axis to predict the cutting force estimation. However, this approach is computationally heavy and not productive. Artetxe et al. [15] included tool run-out by adding a radial offset to the infinitesimal edge element, thus modifying the chip thickness. In these studies, the models considered the uncut chip thickness, and there is a limited dependence on the tool geometry. Layegh and Lazoglu [16] analytically modelled the surface obtained in a 5-axis ball end milling considering lead angles and tool run-out, showing that the tool orientation affects the surface texture. However, the average error obtained on a flat surface was about 20 %. Gou et al. [17] modeled 5-axis flank milling without discretization of the cutting edges. The model included variable helix angle combined with run-out to perform the real trace of 5-axis milling and precisely predict the surface, however, it is not settled so far for free-form milling with ball-end tooltips.

Different approaches can be applied to model the cutter contact between the tool and the surface; the most computer-efficient method is the analytical one, which is very limited and used more for ideal cutting conditions. However, the mathematical model of the surface is protected by the core of the CAD software, and exporting this data is not trivial, so most of all studies regarding ball-end milling of free-form surfaces used monotonic or inclined planes [18].

Discrete and semi-discrete models of the surface are the most commonly used to discretize the cutter workpiece engagement (CWE) during ball-end milling. It is know that the local slope of the surface produces CWE oscillations affecting the cutting speed and oscillating the cutting forces, damaging the process [19]. Thus, discretizing the surface into small and known segments to calculate instantaneous solutions makes it possible to predict point-to-point more complex problems like free-form milling, up to now very limited [20]. Furthermore, some studies have already addressed the CWE calculation using post-processed NC files and the CL data to compute cutting surfaces [21,22], but errors associated with the uneven point distribution are still a limitation, especially for 5-axis machining.

Most of the studies of free-form surfaces are limited to the 3-axis, where the positioning of the tool is always in the z-direction, easing the identification of the pair of CL CC and respective vectors. More complex milling, considering 5-axis toolpath programming, requires detailed information on the tool orientation as well as the surface information. Tunc and Budak [23] developed a methodology for obtaining simulation data in 5-axis milling using CL data generated by CAM software. However, their proposed methodology requires comparing the CAM file with one using the same strategy generated using null tilt and lead angles to determine CC and its respective vector as well as an STL of the surface, which increases pre-work and limits its application to gauge-free surfaces.

The recent growth of Industry 4.0 promotes machines and software integration to predict or control manufacturing processes, but integration with CAD/CAM software is still a limitation [24]. Thus, developing a methodology based on the CAM software, which considers the embedded CAD geometry, to obtain data for modelling 5-axis ball-end milling is still necessary for academic and industrial purposes.

These difficulties lead to the wide use of empirical methods in the shopfloor and confocal microscopy imaging analysis, which is time-consuming. This technique uses microscopy and laser light filters to reproduce the high-resolution surface texture, which is valid for inspection and surface model validation [25]. The accurate evaluation of the topography will reveal vibrational and more complex problems present in the manufacturing process. On the one hand, mixing all the damages makes hard the investigation of individual effects. On the other hand, it allows an accurate topography prediction considering regression with the geometrical model and all the noise obtained evaluating the surface [1].

Another method to evaluate the surface is comparing local results with the theoretical roughness. Although surface roughness has been more representative, lineal roughness is most commonly used to evaluate the surface due to the price and versatility of the 2D rugosimeter (ISO 1302, highlighting the 2D parameters Ra, Rt, Rz). However, it should be taken into account that diverse profiles can display identical roughness parameters and perform mechanically differently [26]. According to Mali and Gupta [27], the surface roughness of ball-end milling can be mathematically predicted with high accuracy regarding the scallop's height. The scallop height measures the height of the highest point of the mark left by the ball-end tooltip and the lowest of the following cutting step. However, this is only valid when the material is sheared from the surface.

Scandiffio et al. [28] evaluated the roughness of a free-form surface after a milling operation using a ball-end tooltip. The authors identified that the roughness is influenced mostly by the CWE and tool wear but did not consider the tool run-out, which is required to obtain a more precise simulation. Urbikain and Lacalle [29] evaluate the effect of the ICE element of end mills on the roughness. They observed that the lead

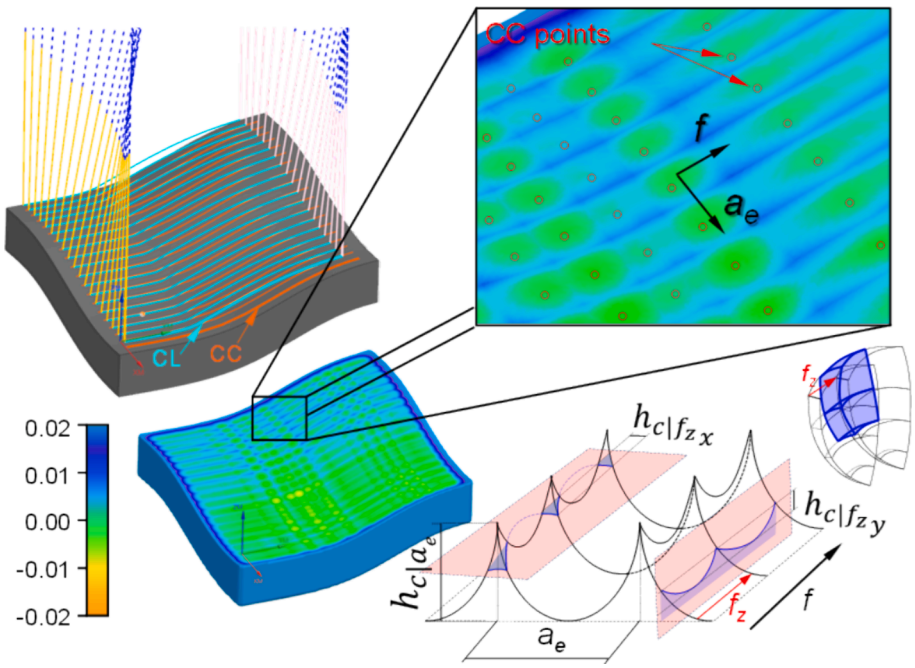

Fig. 1. Typical surface prediction by commercial CAM software.

and helix angles had less influence on the average roughness for this kind of tool, while the tilt angle reduction improves surface roughness.

Another aspect that is highlighted in ball-end milling is the effect of the tooltip. The tooltip can negatively affect the cutting process by increasing the components of the cutting force, increasing the tool wear, modifying the direction of its components, and other related problems that damage the surface. Furthermore, tooltip wear can lead to surface integrity issues, such as roughness, irregularity, and damage to the machined surface that facilitates the corrosion and fatigue process. Optimized feed rate and cutting speed cutting conditions can minimize the tooltip effect but cannot completely eliminate it.

The cutting speed is null at the center and nearby regions, resulting in a cutting phenomenon known as plowing. When the minimum chip thickness is not achieved, the material is crushed instead of sheared. Thus, tool inclination is always preferable to avoid tooltip center contact [30]. However, due to geometrical constraints, sometimes it is impossible to evade the tooltip or nearby regions, resulting in a surface with severe plastic deformation, side flow, scratching, and cavities. Also, several pull-outs and high residual stresses can be found with different magnitudes according to the machined material [31,32]. These marks left on the surface are hard to predict but easy to identify in a post-evaluation with optical imaging analysis. Knowing the idealized surface can improve the identification and a better comprehension of the process. Modeling the finish milling considering the tool's effective radius is essential to include the plastic deformations and a proper surface prediction.

Also, in many studies, the effect of the tool orientation is investigated, mitigating variations in the topography with the tool tilt and cutting direction. Oliveira et al. [33] quantified geometric errors on 4-axis milling of thin-walled parts in up-cutting or down-cutting. The authors attributed the form deviation to the cutting force but did not evaluate the surface roughness and the tool run-out towards advancing the milling process simulation. Chen and Huang [34] studied the surface topography of ball-end milling considering the cutting-edge geometry. The authors evaluated the scallops of the surface for specific tool inclinations. Tilting the tool above 10° propitiated a better surface roughness for most tool diameters. Liu et al. [35] recommend increasing the lead angles up to 45 degrees on ball-end milling to achieve better roughness values. The authors attribute this improvement to the increased effective cutting speed and decreased velocity gradient. Besides, the marks left on the feed direction were about 3 to 4 times more sensitive to tool inclination than the ones left by the lateral passes to the surface roughness.

One way to investigate the quality of the manufacturing process is by directly analyzing the texture left on the machined surface. The milling process has intermittent and repetitive patterns that can characterize the surface and the process. During the cutting, the orientation of the cutting edge changes periodically with the rotation of the spindle and feed and, thus, by the feed per tooth, making periodic marks overtime on the feed direction. These marks are not well predicted in the simplistic simulation tool of commercial software (Fig. 1), making the process prediction and surface evaluations challenging and ruled by empirical knowledge. Besides the inverse cinematic of the 5-axis machining, the complexity of the engagement of the tool with the workpiece and limitations on exporting the surface data make the process modeling difficult for free-form surfaces.

Nowadays, there are some models to predict topographies and other aspects of the milling process that include forces and their derived problems. However, there are many limitations when free-form surfaces and 5-axis milling are involved due to several data inputs required and boundary conditions. Additionally, studies with free-form surfaces usually use ball-end tooltips that result in more complex geometric problems, requiring surface data for modeling that is usually protected by the CAD/CAM software. So, it is common to find limited or idealized studies with specific geometries, contact conditions, or cutting parameters.

To obtain a robust milled model to predict the texture of free-form surfaces, including material properties, the effective cutting speed of the tooltip, feed rate oscillation, tool run-out, cutting parameters, as well as cutting geometries and CWE geometrical model, is necessary. In this context, the current work proposes modeling and investigating the surface texture left after free-form milling with conventional ball-end tooltip. Considering the crest height on the feed direction. Therefore, a methodology for computing free-form surfaces is proposed based on the discretization of the toolpath obtained by a post-processed NC file, improving the CAD/CAM estimation and boosting industrial applications. Furthermore, a routine is developed to obtain data for general 5-axis milling of free-form surfaces, using this data for surface prediction

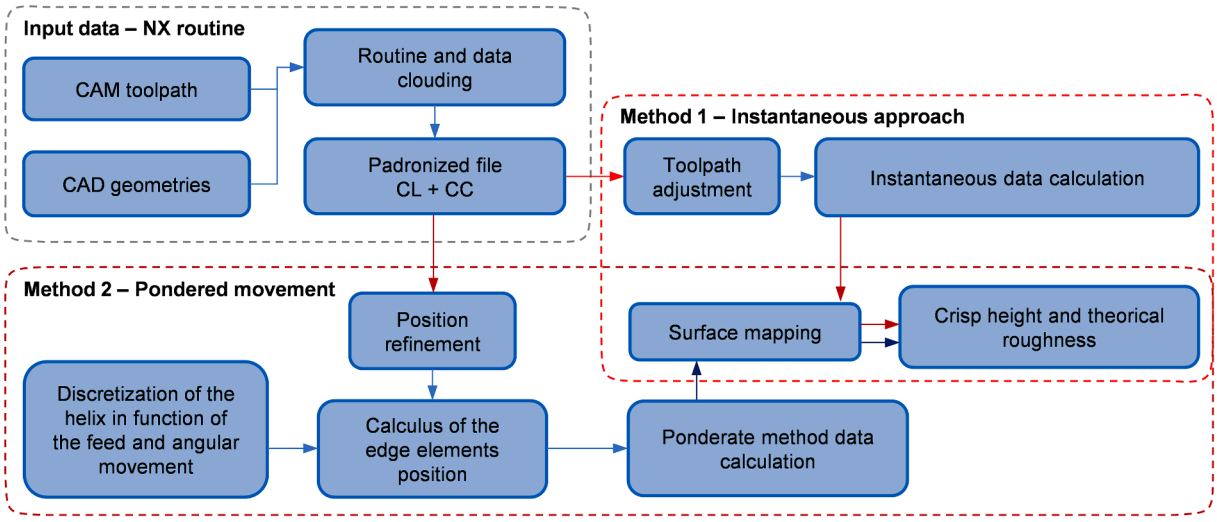

Fig. 2. Flowchart of the proposed methodology for surface prediction.

and easy future evaluations of more complex problems that require geometrical data of the tool and the surface.

2. Materials and methods

Considering the limitations of the current CAM software of simulating the real texture of a machined surface, predicting the cutting force and the geometric errors, among others, the present work presents a new approach to obtaining information directly from the CAD/CAM software by the CAD geometry and the toolpath (CC and CL data) which can be used for further developments. The current study employs this methodology to predict the machined surface texture for milling free-

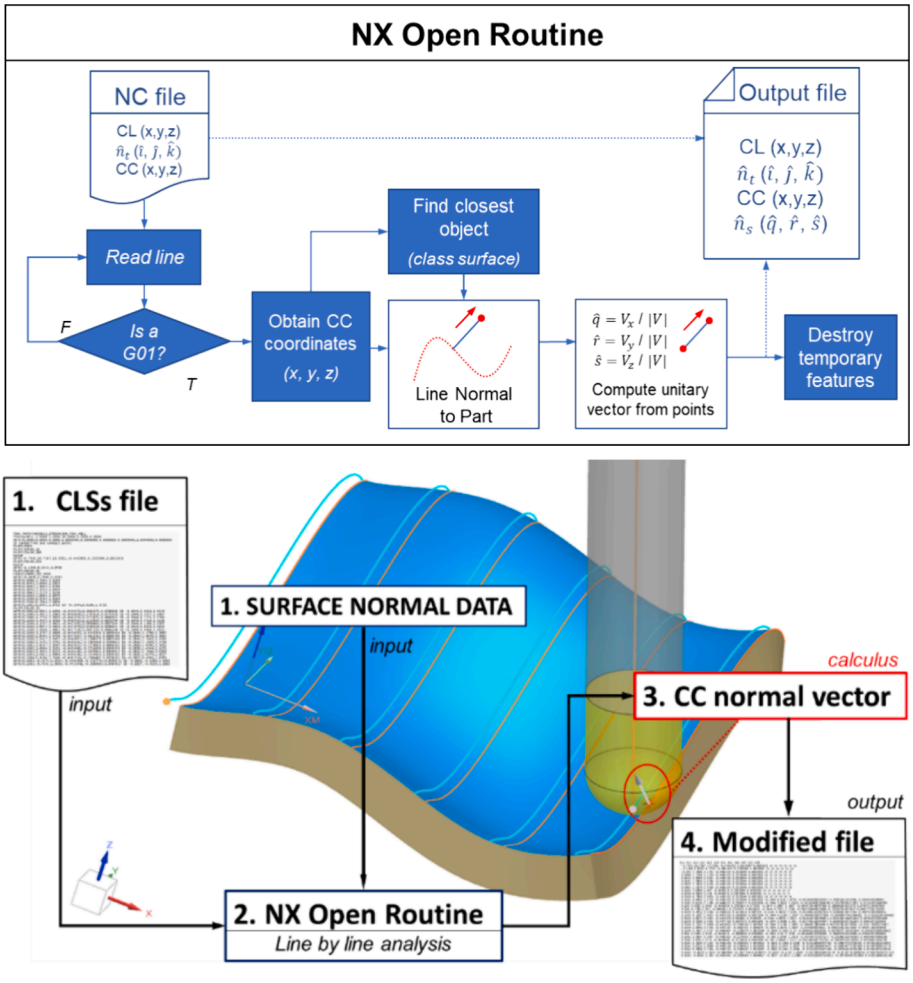

Fig. 3. NX Open routine schematic and flowchart.

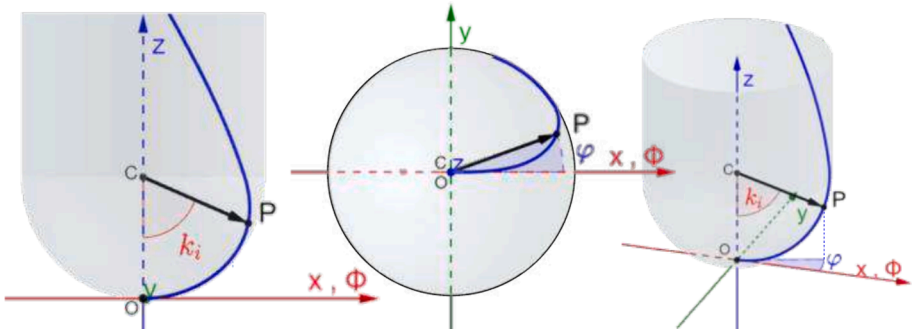

Fig. 4. Tool schematics for single radius tooltips.
Source: https://www.geogebra.org/m/hkdr6rhj

form shapes in 5-axis machining.

The methodology consists of discretizing the complex surface during a 5-axis milling operation and calculating the tool and surface instantaneous positions along the toolpath. This approach can also be extended to predict more complex problems dependent on the force, considering both CL (Cutter Location) and CC (Contact Condition) data.

The proposed development was organized into six topics. First is presented a (2.1) overview of the proposed methodology, then the (2.2) routine for data collection developed in the software Siemens® NX is described, followed by the (2.3) geometrical modeling of the tooltip, (2.4) toolpath data treatment, and (2.5) surface prediction is presented with two modeling approaches. The first one considers the instantaneous position of the tooltip to predict the surface texture. In the second one, the trajectory of the infinitesimal elements of the tool are taken into account to improve the lateral roughness prediction of the milling process. In both cases, the effect of the tool run-out was considered. Finally, the materials and methods for evaluating the implemented routine and the mathematical modeling are presented (2.6).

2.1. Proposed methodology

A programming routine was developed to obtain a set of data necessary for modeling the surface. The first step of the proposed methodology is obtaining any complex surface's cutting contact (CC), cutting location (CL), and respective normal vectors by an implemented routine on the CAD/CAM software. A standard language C#, was used in the programming routine because it is compatible with the open interface (NX Open) of the software used – Siemens® NX. It is worth noting that the same methodology can be adapted to other software programs that have an open programming interface.

Then, a geometrical model was developed based on the routine outputs to predict the ball-ended cutting-edge movement and the surface of 5-axis milling. In this second step, the geometries of the tool were mathematically modeled with a scope limited to ball-end tooltips with a constant helix angle. In this step, two approaches were considered. The first considers the dome after a complete rotation of the tool (instantaneous position), and the second one considers the trochoidal movement of the instantaneous cutting-edge (ICE) element (pondered movement), which allows to include, i.e., the tool run-out. After that, both data were used for surface texture evaluation, measuring topography, scallop height, and theoretical roughness. Fig. 2 presents the flowchart of the proposed methodology.

2.2. Routine for data collection

For surface mapping, a routine was developed using an API (application programming interface) on the software Siemens® NX 1953 to obtain a list of the cutting location (CL), cutting contact (CC), and respective vectors. These data were obtained following a series of procedures in accordance with the developed routine.

The first requirement is importing or modeling the workpiece geometry in the software, followed by the usual CAM programming. Thus, both geometry and trajectory will be available for computation and posterior milling. As a second requirement, it obtains the post-processed NC program file in the standard format (Cutter Location Source File – CLSF), providing normalized data to the routine containing the CC and CL data. In the case of the Siemens® NX software, the CC data were obtained through CAM post-processor once the output Contact Data is enabled. Then, with the path and directory of the exported CLSF file or the data extracted directly by the software routine, a series of filters and sorts are done while the output data missing is computed line-by-line – the surface normal vectors for a given contact point.

An NX command was used to obtain the vector normal to the surface on a specific CC location. The command input requires a surface and a point to calculate the normal direction. Thus, a specific CC point is used for selecting both the position and the surface. The surface selection was automated by selecting the feature object closest to its specific CC point. Finally, the unitary vector related to the CC is calculated using a support line with its respective extreme points, and then all the features involved are destroyed; this procedure is detailed in Fig. 3.

Highlight that most CAD/CAM software has closed architecture, so obtaining data relative to the surface in a specific position is not trivial. At the end of the calculation, all the non-cutting moves lines are filtered, and the other lines are presented in a standardized file with 12 columns. The first three columns represent the x, y, and z coordinates related to the CL points, columns 4, 5, and 6 present vectors $\hat{i}$, $\hat{j}$ and $\hat{k}$ (related to the tool orientation), columns 7, 8, and 9 represent the x, y, and z coordinates of the respective CC points, and the last three columns represent the $\hat{q}$, $\hat{r}$, and $\hat{s}$, vector normal to the surface on a given CC point, as exemplified in Fig. 3.

2.3. Geometrical modeling of the tooltip

For the tool modeling, a reference system was defined using the right-hand rule and the center of the tooltip, with a clockwise rotation on the tool axis, as depicted in Fig. 4. Then, the tool is mathematically modeled. The local radius is calculated according to the tool's height. Then, the axial and radial immersion angles are calculated to describe the edge position inside the tool's dome. Finally, the effect of the tool run-out in ball-end tooltips can be included as a function of the tool's height – $r(z)$. Fig. 4 presents the ball-end tool schematic.

Considering the given reference system at the end of the tooltip, Eq. (1) gives the coordinates of the dome of a ball-end tooltip.

$$\begin{cases} x_i = R sin(k_i) sin(\theta_i) \\ y_i = R sin(k_i) cos(\theta_i) \\ z_i = R - R cos(k_i) \end{cases} \quad \text{for } 0^\circ \leq k_i \leq 90^\circ \tag{1}$$

Where R is the radius of the tool, k_i is the axial immersion angle adjacent to the vertex C (0, 0, R), shown in red in Fig. 4. For a given angular position θ_i, k_i defines the position of the point P along the tool

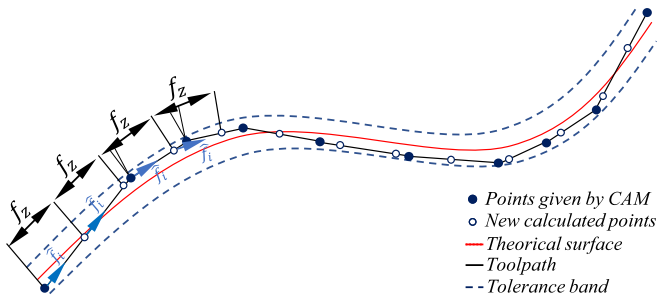

Fig. 5. Center deviation caused by run-out at a generic zi plane of the tool.

helix using Eq. (1).

To model the cutting edge, infinitesimal elements i must be defined as a function of the height. Considering that the angular position increases as the height increases, a helix can be defined at the tool dome. Defining an angular reference $\varnothing$ measured from the X-axis and the angular increment with height as φ_i, it gives the angular position θ_i, Eq. (2).

$$\theta_i = \varnothing - \varphi_i \tag{2}$$

Where the angular increment with height φ_i is defined by the tangent at a given point with a plane perpendicular to the tool axis, Eq. (3).

$$\tan\alpha = \frac{R\Delta\varphi}{\Delta z} \therefore \tan\alpha_i = \frac{R_i\varphi_i}{z_i} \tag{3}$$

Considering that the ball-end tooltip has a constant helix angle, the infinitesimal edge increment with height can be expressed by Eq. (4).

$$\varphi_i = (1 - \cos k_i)\tan\alpha \tag{4}$$

Combining Eq. (1) to Eq. (4) is possible to define the edges of a ball-end tooltip with a constant helix angle.

Run-out ρ involves both manufacturing errors and clamping miss alignment of the tool-holder system. It can be described as a function of the local radius with the height, Eq. (5), thus dependent on the micro edge element and reliant on angular position and axial immersion angles.

$$r_j(z) = r(z) + \rho(z) \tag{5}$$

Where $r_j(z)$ is the local radius of the micro edge element related to the j flute, $r(z)$ is the local radius of the tool, and $\rho(z)$, the radial deviation of the respective micro edge element depends on the element's position in the space. Considering an ideal manufacturing process for the tools, $\rho(z)$ can be approximated to a linear function with a reference system as an offset (in the xy plane) and tilt (τ) from the reference tool axis, Eq. (6).

$$\rho(z) = \rho_0(x,y) + f(z,\theta) \tag{6}$$

Fig. 5 instantaneously exemplifies the linear movement of an infinitesimal edge element i with the effect of the tool run-out on the top view. Additionally, other factors, such as initial tool wear and thermal expansion, can be modeled similarly as a function of the local radius but are not considered in this work.

Fig. 5 shows that in the milling process with run-out, it is possible that only one tooth generates the surface, so it is proposed a simple calculation to adjust the surface prediction based on the feed-per-tooth, tool run-out, and the number of teeth. The logic consists of comparing the bigger effective radius ($r_1 = r_{max}$), subtracting the theoretical crest wave (h_c) and comparing it to the other teeth; if the value of the effective radius is smaller, it will not participate in the surface generation. Also, the index number of those teeth must be saved for plotting. The average distance of the surface feed-per-tooth mark is given by Eq. (7).

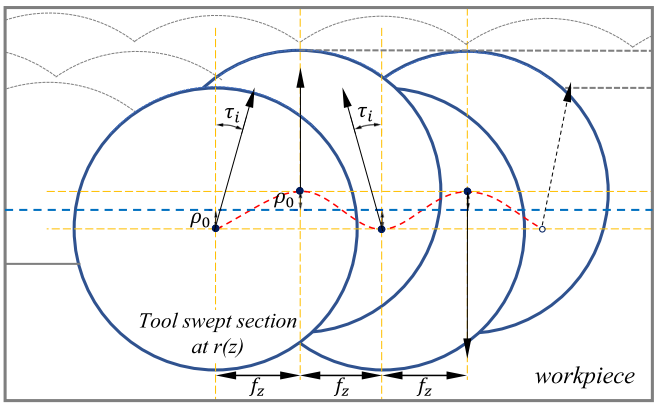

Fig. 6. Schematics of toolpath adjustment for surface prediction considering instantaneous positions.

$$\overline{f_z} = f_z\left(\frac{z}{z_c}\right) \tag{7}$$

Where z_c is the number of teeth participating in the surface generation, given by Eq. (8).

$$z_c = \sum_{i=1}^{z-1} 1 + i : \{i = 1 \text{ if } r_z > r_1 - h_c;\ \text{else } i = 0\} \tag{8}$$

2.4. Toolpath data treatment

Using the tool geometry (section 2.3) and the toolpath generated by the CAD/CAM (section 2.2), with two procedures, it is possible to predict the surface with an error lower than the tolerance band used in the toolpath generation. The first is calculating the instantaneous positions, pondering the known contact positions (2.4.1). The second one is computing the angular position of the cutting-edge element according to the tool tilt and toolpath data (2.4.2).

2.4.1. Instantaneous position evaluation

Usually, the spindle speed is much higher in the milling process than in the feed, making the spindle speed effect on the surface topography higher than the feed per tooth [36]. So, it is possible to consider that a complete rotation happens instantly, removing the material. However, in a discrete model, this assumption leads to an additional error associated with the difference between the segment's lengths from the feed-per-tooth (f_z). Thus, a good correlation between these parameters is important for the model's accuracy. When the segment length is bigger than the f_z, more material is removed, while when f_z is bigger, the material is underestimated. Otherwise, it is necessary to calculate intermediary points to discretize the movement.

Naturally, on complex surface milling, the distance between the NC points changes depending on the surface's tolerance band and local curvature. So, it is necessary to interpolate the mapped surface data obtained by the routine according to the f_z used to increase modeling accuracy. Fig. 6 presents a schematic of the method applied to compute intermediary points using the CL and its respective tool orientation.

In the process of discretizing intermediate positions, their respective unitary vectors are also calculated. It is known that the unitary vector of the tool position ($\hat{n}_t$) obtained from the processed 5-axis CL file can be written in terms of $\hat{i}\ \hat{j}\ \hat{k}$ positions given the orthogonal cartesian components relative to x, y, and z, Eq. (9).

$$\hat{n}_t = n_x\hat{i} + n_y\hat{j} + n_z\hat{k} \tag{9}$$

The data obtained using the routine gives the instantaneous tangent plane of the surface, described by the respective point CC and the unitary vector $\hat{n}_s$, Eq. (10).

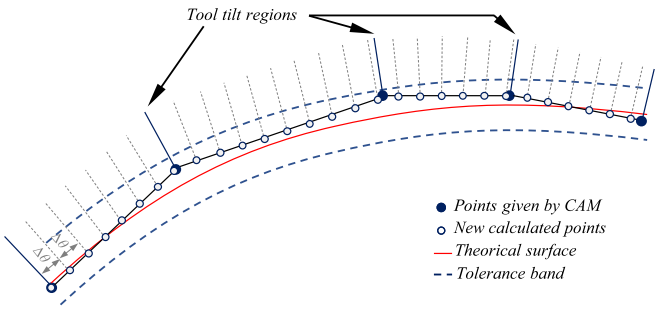

Fig. 7. Schematics of toolpath discretization with a constant Δθ and tilt ponderation.

$$\hat{n}_s = n_x\hat{q} + n_y\hat{r} + n_z\hat{s} \tag{10}$$

To calculate the instantaneous direction ($\hat{\hat{f}}_i$), the product of the unitary vectors relatives to CC and CL is computed, Eq. (11). And by the cross-product of the tool position with the local surface vector, Eq. (12), it is obtained the instantaneous lateral pass $\hat{g}_i$.

$$\hat{f}_i = \frac{\hat{n}_s \times \hat{n}_t}{|\hat{n}_s \times \hat{n}_t|} \tag{11}$$

$$\hat{g}_i = \hat{n}_s \times \hat{n}_t \tag{12}$$

2.4.2. Adjustment of the angular position with the toolpath

If the spindle speed is not considerably higher than the feed or a better estimation is required, the angular position of the tool edge must be considered. Additionally, cutting-edge orientation is required to include the effect of the tool's helix and the run-out on the surface estimation. Thus, an additional procedure was developed, adjusting and synchronizing the angular position with the feed (axial movement of the tool). Equation (13) expresses the angular position in terms of the nominal feed per tooth, which allows the computation of the angular position for each CL (or intermediary points) according to the tool's displacement.

$$f_z = \frac{\Delta dT}{t_{i+1} - t_i} = \frac{\Delta d}{t_{i+1} - t_i}\frac{2\pi}{\omega} \tag{13}$$

Where Δd is the distance between consecutive CL points, T is one rotation period, ω the angular velocity, and t_{i+1} and t_i are respectively the intermediate and the initial position during one rotation.

Considering that the tool has a constant angular speed (ω), it is possible to indirectly correlate the feed distance covered with the angular position (θ). Splitting the toolpath into constant intermediary points will also result in a constant Δθ. With this consideration and knowing the total distance covered by the tool, it is also possible to obtain the angular position of any micro edge elements on the toolpath. Fig. 7 presents a 2D schematic of a Δθ weighted interpolation between the CL points.

However, when new data points are generated, it is necessary to compute the related tool's tilt. It is done by adjusting to the previously known unitary vectors and pondering with known positions. Furthermore, in both methods presented, instantaneous or pondered movement interpolation, the data created can be used for any surface. In the specific case of angular interpolation (Δθ), the discretization process is more critical and must be optimized to obtain a good correlation between the precision and the computational time. The smaller the Δθ, the better the precision, but the higher the computational time. Thus, the trochoidal toolpath of the ICE elements can be graphed using polynomial regressions (cubic spline) to improve processing time and maintain accuracy.

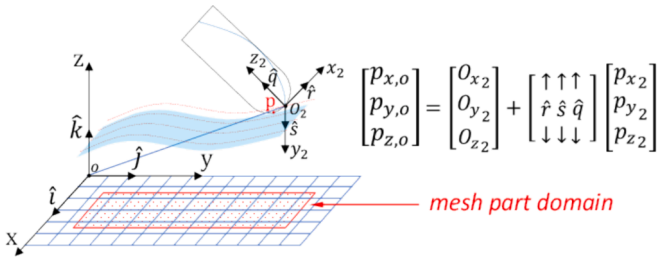

Fig. 8. Geometrical rotation and translation procedure applied to tool dome and infinitesimal edge elements.

2.5. Methodology for surface evaluation

First, the data were sorted according to the part's world coordinate system (WCS) for easy graphical visualization and evaluation of the surface. To do so, a mesh at the *xy* plane was created considering the maximum and minimum positions of the NC code, leaving the high in *z* to be computed considering the instantaneous positions and the pondered movement of the tool. For each specific position, the minimum (or maximum) *z* hight is computed. The tools dome or infinitesimal edge element was translated and oriented according to (WCS) using the procedure described in Fig. 8. Hereafter, each geometrical feature was oriented according to the data obtained by the routine and optimized with the procedure presented in the previous section, obtaining the *z* height for each mesh position.

Then, two different methods were applied to inspect the surface texture. The first was a simple evaluation of the scallop height to measure the theoretical roughness in the feed direction. The second is using the data cloud of the surface to compute the theoretical surface.

2.5.1. Scallop height considering instantaneous positions of the tool

In order to obtain a local estimation of the surface, a simple model to calculate the scallop height is applied. It can be directly associated with the roughness and indirectly to measure the quality of the milling process. The tool's geometry and cutting parameters feed-per-tooth (f_z) can be used to estimate the theoretical roughness of the surface considering the instantaneous positions (discretized toolpath), Eq. (14). The scallop height (h_c) also can be used to calculate the roughness R_z trought Eq. (15) [37–39].

$$h_c = R\left(1 - \sqrt{1 - \left(\frac{f_z}{2R}\right)^2}\right) \tag{14}$$

$$R_z = \frac{\sum_{n=1}^{5} R_{zn}}{n} \tag{15}$$

To apply these equations throughout the 5-axis trajectory, the discretized model is used to calculate the deviations in relation to the instantaneous cutting plane for each position. Thus, the deviations are obtained as a function of the local inclination of the surface and a good approximation of the actual surface roughness.

Knowing that the center of the tool has a low cutting speed and the plowing cutting phenomena is dominant, two regions were evaluated, the first in the central toolpath region where the center acts in the cut and another with a higher specific cutting speed, both on the feed direction.

2.5.2. Surface prediction using the mesh data cloud

Translating the tool position and plotting the minimum z distance for each position of the equally distributed data cloud allows the simulated surface to be obtained. Then, the data were compared with confocal microscopy results of the curved surfaces (concave and convex regions) and with the form removed by Leica Map 6.2 software. Likewise, the toolpath of an infinitesimal cutting-edge element was plotted according

Table 1
Composition of Waspalloy- AMS 5706.

Ni	Cr	Co	Mo	Ti	Fe	Al	Zr	C	Mn
58.64	19.34	12.27	3.82	3.04	1.35	1.33	0.05	0.04	0.03
Si	**Cu**	**B**	**Mg**	**P**	**N**	**S**	**Se**	**Pb**	**Ag**
0.03	0.02	0.005	0.005	< 0.001					

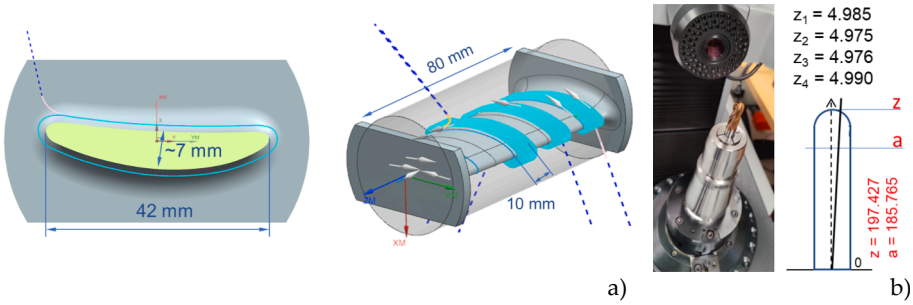

Fig. 9. a) Part model and machining strategies. b) Presetting results.

to a specific height, obtaining the trochoidal movement of the ICE element. The smaller the $\Delta\theta$ used for computation, the higher the precision of the trajectory of the element.

2.6. Case study experimental procedure

A bladed shape part containing free-form concave and convex surfaces was designed using the software Siemens® NX and manufactured to evaluate the proposed methodology. The material used was a solid bulky cylinder with a nominal diameter of 46.5 mm of Waspalloy AMS 5706, the nominal composition presented in Table 1. The machine used to manufacture the blade was a multitask machining center Mazak i200 with smooth machining configuration (SMC) by default (balanced). The milling experiments were conducted utilizing the machine's tailstock.

The blade was finished using a ball-end tooltip with a 5 mm radius manufactured in micro grain solid carbide with 10 % Co coated with

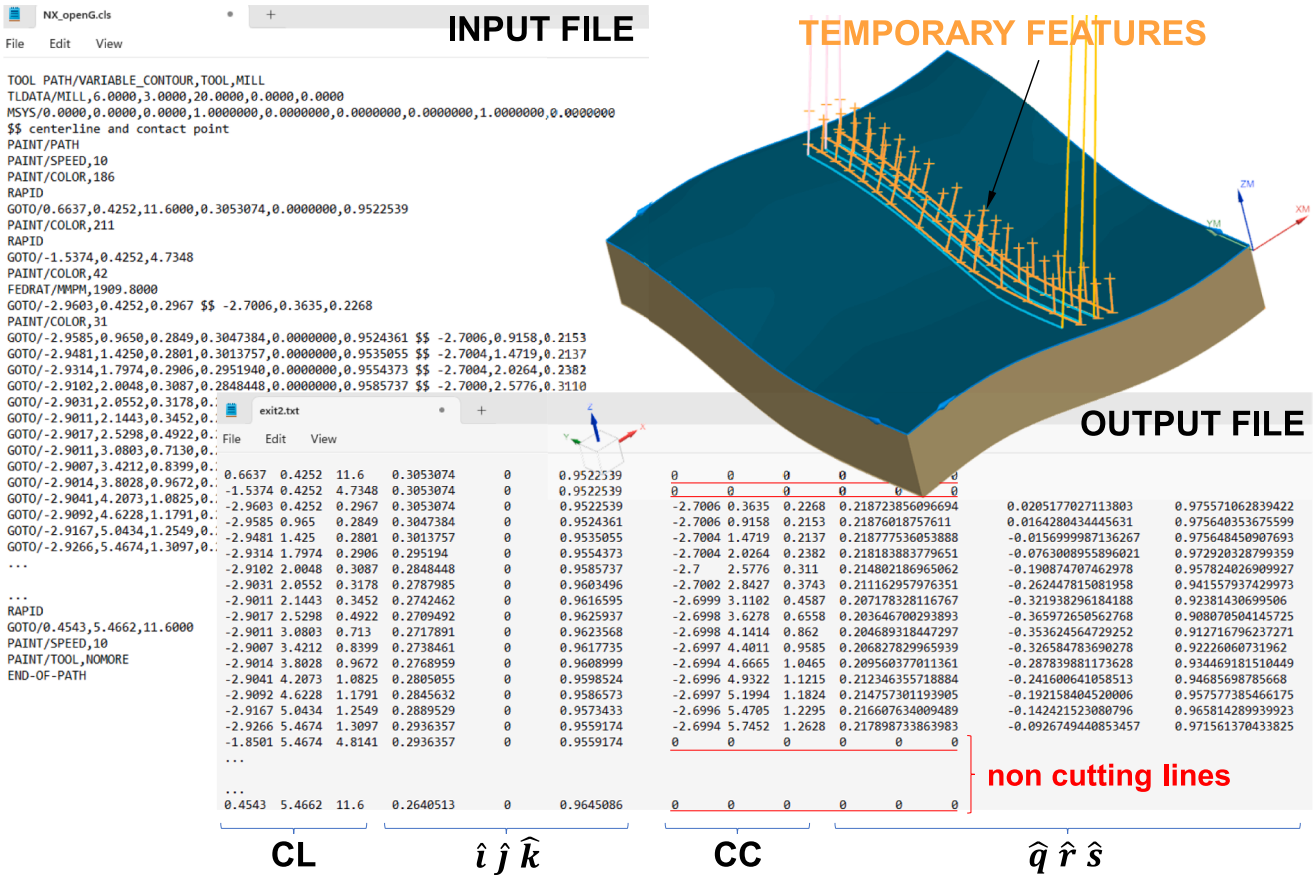

Fig. 10. Programmed routine for 5-axis data acquisition outputs.

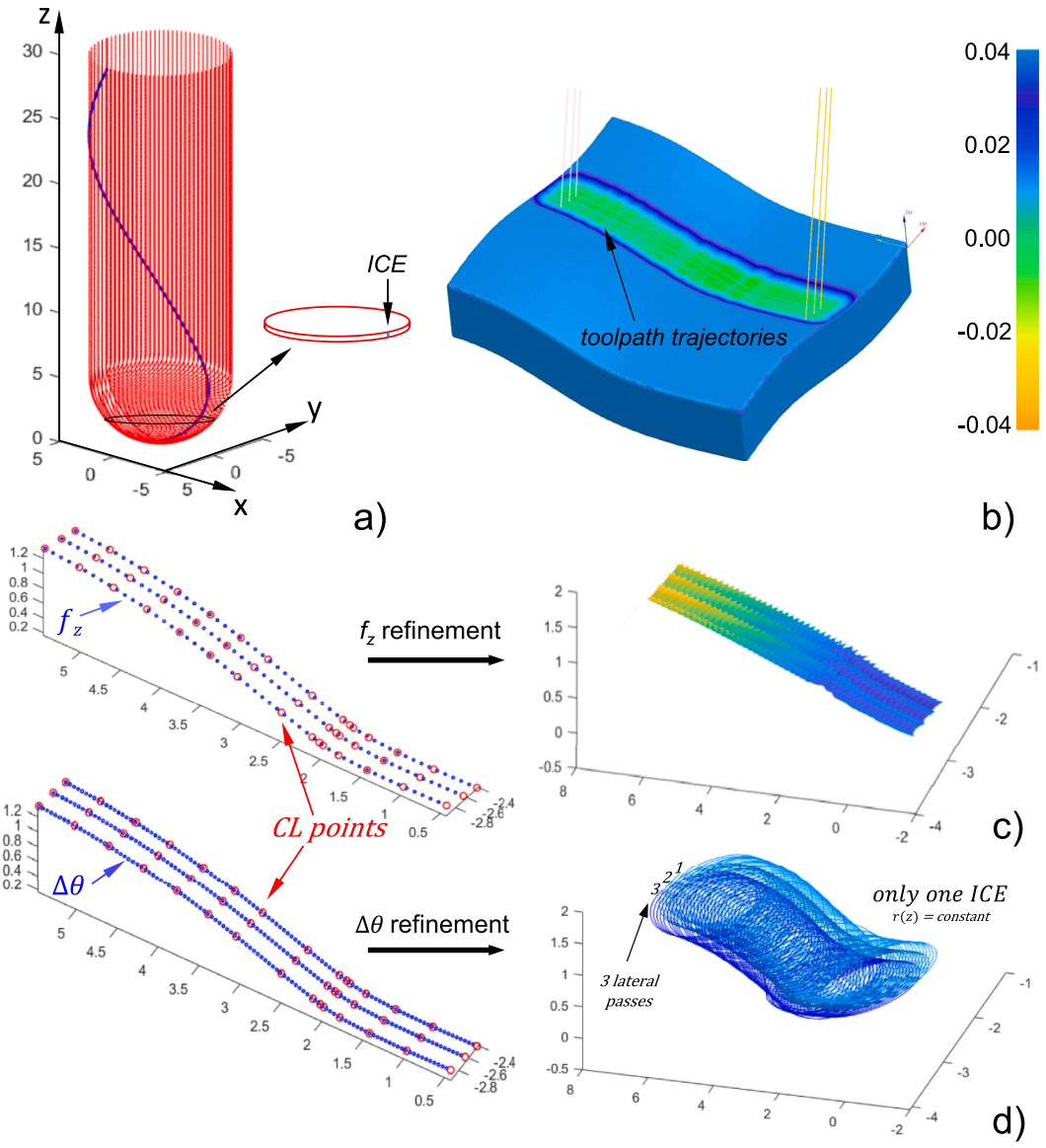

Fig. 11. a) Ball-end tool dome and helix edge; b) 5-axis milling on a free-form surface simulated by the cam software; c) toolpath data treatment for instantaneous surface modeling and application; d) toolpath data treatment for ice trochoidal movement and application.

multilayer TiSiN (3800 HV 0.05) with four flutes and a 30° helix angle. The tool was mounted on a high-torque tool holder with a 40 mm cantilever, and a presetter Zoller® SmarTcheck 600 was used to measure tool length and the static run-out, as depicted in Fig. 9b.

The milling trajectories were programmed on the software Siemens® NX, considering rough, semi-finishing, and finishing operations. A spiral toolpath with 0.4 mm of a_e was used in the semi-finishing operation, leaving the part with 0.4 mm stock for the finishing operation. The finishing process was conducted in down-milling with constant a_p (0.4 mm), a_e (0.2 mm), f_z (0.05 mm/tooth), and cutting speed of 80 m/min (parameters recommended by the tool maker). Then, three different regions with 10 mm lengths were evaluated using, in all of them, a 5-axis spiral strategy (with a 0.01 mm tolerance band). This strategy avoids tool entrances and exits that damage the surface and compromise its integrity. Also, the direct action of the tooltip was avoided by tilting the tool in the feed direction. Three cutting engagements were assessed, one in each region, 5, 15, and 25 degrees, respectively. Fig. 9a depicts the toolpath strategies.

The procedure presented in section 2.5.2 was applied to inspect the manufactured parts. A confocal microscope Leica® DCM3D together with the software Leica® Map 6.2, were used for surface visualization, roughness measurement, and data cloud exportation. The surface data was treated using Matlab® 2021 software to compare the values with the simulation predictions using the proposed model. During the data treatment, the surface was analyzed as scanned and without form, where a 5th-order polynomial regression was used to ease the roughness and model evaluation.

3. Results and discussions

The proposed methodology and implemented routine to extract data for predicting and evaluating free-form surface manufactured by milling is presented as follows: 3.1 Routine outputs, 3.2. Data treatment and model output; and 3.3 Study case results and modeling evaluation.

3.1. Routine outputs

Fig. 10 presents an example of a 5-axis toolpath program and the results obtained using the developed methodology. As can be seen, the figure presents the temporary features (lines and points) used to support

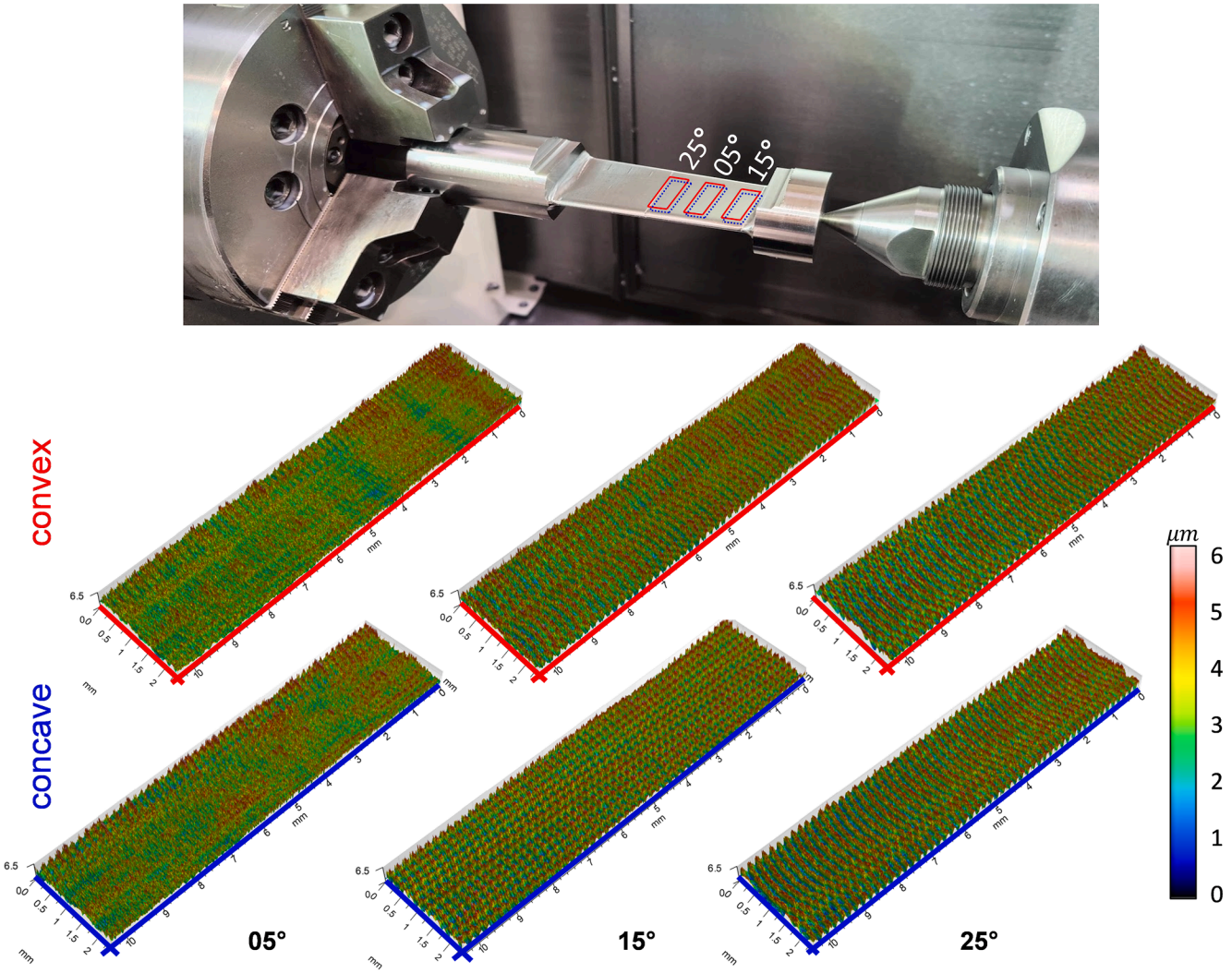

Fig. 12. Machined blade and topography inspection of the central region.

the computation of the normal vector at the CC location and the output data (CL, CC, and respective vectors of the tool and surface). The output file also shows that the non-cutting lines can be identified through the null values of CC and surface normal vector columns. However, depending on the software used for posterior analysis, it can change to NA or N/A.

During the development of the routine, it was observed that the graphical representation of features and part rotations consumes a lot of computational resources, making the routine slow. Thus, in a depuration step, camera rotations and the graphical plottings of the temporary features were suppressed.

3.2. Data treatment and model output

Fig. 11 presents an example of the results obtained using the geometrical model developed together with the routine data output. Fig. 11a presents the geometrical model of the ball end tooltip considering the dome and the infinitesimal cutting edge element according to the tool's height $r(z)$. Fig. 11b presents a 5-axis toolpath trajectory and the topography simulated by the software Siemens® NX. Then, two approaches for data treatment and milling process evaluation are presented. The first is by computing intermediary data according to a specific feed-per-tooth aiming the topography prediction using the instantaneous position procedure (Fig. 11c). The second procedure, depicted in Fig. 11d, discretizes the lineal toolpath into constant $\Delta\theta$ and uses this data to compute the toroidal toolpath of the ICE (pondered movement). Even though the instantaneous position method is simpler, the pondered movement procedure allows a more precise prediction of surface texture, especially in the lateral feed direction. Additionally, the detailed movement of each ICE allows including the tool run-out, enhancing the prediction of surface roughness and topography. The study case of the manufacture of a blade in Waspalloy AMS 5706 using continuous 5-axis milling with a ball-end tooltip and the inspection regions, respectively, to the lead angles of 5, 15, and 25 is presented in Fig. 12, together with the evaluation of the machined surface by confocal microscopy.

Fig. 13a and b present the roughness profile results measured for all cases evaluated with two samples for each condition obtained by confocal microscopy, allowing the evaluation of the cusp marks on the feed direction, respective roughness, and characteristic noise that comes from tool scratches (tool wear or imperfection), plastic deformations, and tool run out.

Table 2 summarises the results of the roughness Ra and Rz of the profiles measured by confocal microscopy depicted in Fig. 13a. It can be seen that the roughness is higher on the convex side for all cases evaluated, a fact directly related to geometrical factors of the surface curvature of the part and CWE, which contributes to convex and reduces on concave surfaces. Also, it was observed that the roughness increases with the increase of the lead angle. Taking into account that only the ball dome acts in the cut (the same geometry for all tilts) and evaluating the

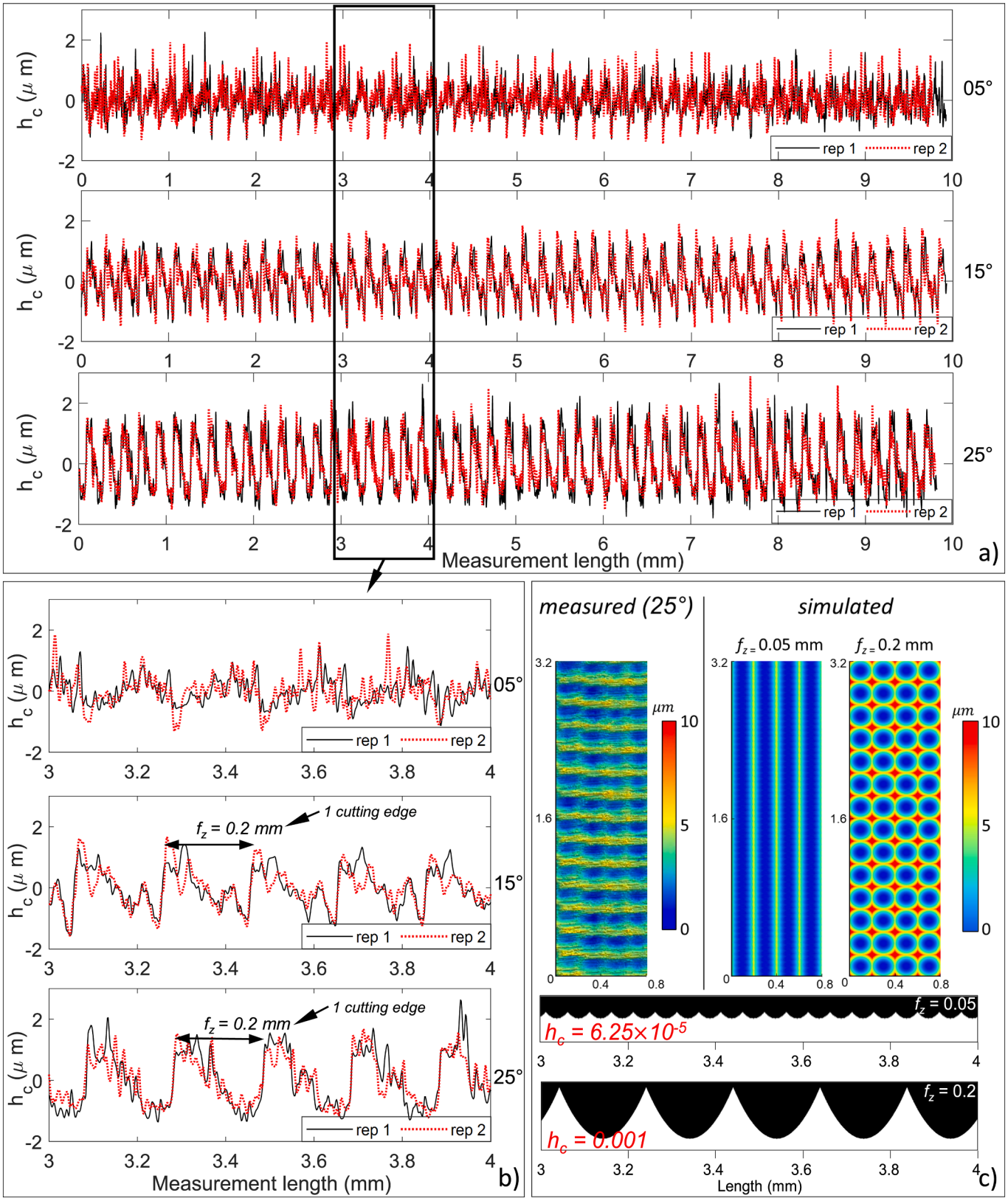

Fig. 13. Roughness and topographical analysis: a) measured roughness profile; b) profile evaluation; c) comparison between simulated and measured with 25° lead angle.

Table 2
Surface roughness obtained by confocal microscopy.

Lead angle (°)		Concave			Convex		
		5	15	25	5	15	25
***Ra* (μm)**	**S1**	0.314	0.418	0.596	0.403	0.499	0.625
	S2	0.333	0.437	0.513	0.459	0.441	0.502
	$\bar{x}_{Ra}$	0.324	0.428	0.555	0.431	0.470	0.564
	σ_{Ra}	0.013	0.013	0.059	0.040	0.041	0.087
***Rz* (μm)**	**S1**	2.07	2.20	2.65	2.55	2.77	2.82
	S2	2.29	2.59	2.60	2.36	2.43	2.67
	$\bar{x}_{Rz}$	2.18	2.40	2.63	2.46	2.60	2.75
	σ_{Rz}	0.16	0.28	0.04	0.13	0.24	0.11

Table 3
Lead angle effect on the effective radius and cutting speed (a_p of 0.4 mm).

	Lead angle (°)		
	5	15	25
Vc_{ef} max(%)	47.1	61.7	74.4
R_{ef} max (5 mm)	2.353	3.083	3.720
R_{ef} max (z1) – 4.990 mm	2.3501	3.0788	3.714
error (%)	0.0012	0.1479	0.1634
R_{ef} max (z2) – 4.985 mm	2.3487	3.0765	3.7109
error (%)	0.1853	0.2219	0.2451
R_{ef} max (z3) – 4.976 mm	2.3461	3.0724	3.7054
error (%)	0.2966	0.3551	0.3922
R_{ef} max (z4) – 4.975 mm	2.3458	3.0720	3.7048
error (%)	0.3089	0.3699	0.4085

surface texture, it can be inferred that the plastic deformation and elastic recovery of the milling process were the main causes of roughness increase with lead, corroborating with reported by some authors [31,32]. It is also important to add that a higher lead angle and, consequently, higher effective cutting speed promote plowing reduction [40]. The different effective cutting speeds are presented in Table 3 and help support the hypothesis of the roughness increase with lead.

3.3. Case study

The Roughness *Rz* presented in Table 2 was used to evaluate the simulated topography obtained with the instantaneous position procedure. The simulated surface presents repetitive marks that lead to repetitive samplings during *Rz* calculation, and its mean is equal to the crest height ($Rz = h_c$). Therefore, the roughness *Rz* of the blade surface without form was compared with the h_c of the idealized surface on the feed direction, assuming an error of 8.3×10^{-5} associated with the spiral pass. The theoretical and simulated h_c of 0.0625 μm obtained for a feed-per-tooth of 0.05 mm/tooth was much lower than the measured (about 2.5 μm), indicating the presence of more problems like tool run-out and plastic deformations.

The evaluation of the milling surface (Fig. 12) and the roughness profiles (Fig. 13) of the six surfaces (3 concaves and three convexes) allowed the identification that 5 degrees lead angle did not produce the characteristic intermittent marks of the milling process related to the feed-per tooth. In this specific case, the surface has several scratches and random marks that characterize plastic deformation, probably due to low effective cutting speed (Table 3). Surprisingly, it was also the one with lower roughness, with crest heights of about 2.5 μm on the concave side and 1.9 μm on the convex side. Probably, a combination of factors such as high feed per tooth, lower run-out at the tool center (and its oscillation on a plane close to the surface normal), and stable clamping systems propitiate a smoother surface. Moreover, it highlights that even though the center does not participate in the cut, its nearby region and reduced cutting speed supposedly propitiate a controlled plastic field that improves the final milled surface. However, concerns about the tool wear and higher forces on the z direction must be deeply addressed.

The surfaces manufactured with 15 and 25 lead angles presented clear peaks and valleys. However, the marks were not as distant as the programmed feed-per-tooth (0.05 mm/tooth) but by 0.2 mm/tooth, implying that the run-out was present in the process. This resulted in a deep investigation of the tool run-out. Hence, to improve the surface prediction, the methodology to identify and correct the feed-per-tooth that generates the surface was applied, Eqs. (7) and (8).

First, the difference in the effective cutting radius was calculated for all cases evaluated. Table 3 presents the computed maximum effective cutting speed according to the lead angle and tool run-out. It can be seen that the difference between radii bigger than the theoretical crest height implies that only the major radius will directly generate the final surface. Thus, a feed-per-tooth correction was done to improve the surface prediction, increasing the simulation parameter f_z to 0.2 mm/tooth. The improved result of the surface prediction is depicted in Fig. 13c. It is important to highlight that even though only one tooth generates the final surface, the others act in the cut (if $a_p >$ teeth run out), promoting a gradual removal that can affect the cutting process and surface topography.

As presented in Table 3, the proportional cutting speed in the case of a 5° lead angle is reduced by more than half, affecting the cinematic energy that propitiates shearing and increasing the plowing phenomena, gradually lowering at 15 and 25 degrees, respectively. Furthermore, it was also observed that the lead angle tends to magnify the difference between the radius increasing the tool run-out together with the effective cutting speed. As tilting increases, the difference increases, affecting the roughness, which is one of the main factors that justify the roughness increase from 15 to 25.

Still, with the simulated topography for 0.2 mm/tooth, the crest height observed was about four times lower than the measured by confocal microscopy independently of the surface curvature (concave or convex region). This can be attributed to the plowing effect and elastic recovery of the surface, which cannot be predicted by the geometrical models of the surface. Fig. 14 compares at six different tool heights the trochoidal movement of 4 different ICE elements with the equivalent diameter measured on the Zoller presenter (Fig. 9b), allowing the evaluation of the effect of the three different levels of tilting 5, 15, and 25 lead angle degrees together with the tool run-out present on the machining process.

Fig. 14b presents a top perspective of the cutting, grouping the ICE by the tool height ($r(z) = l_i$). The first that can be noted is that the lateral cusp height decreases as the tool height increases. Secondly, the difference between the lateral crest height using two feed-per-tooth (f_z) levels, 0.05 and 0.2 mm/tooth, can be observed. The four times magnification of the feed-per tooth produced a significative decrease in the roughness, from about 19 to 14 times with the lateral crest height in the first three levels presented (l_2, l_3, and l_4), respectively, 10, 20 and 30 % of the theoretical crest height on the feed direction (considering the effective $f_z = 0.2$ mm/tooth), highlighting the importance of measuring the tool run-out for a correct estimation of the effective f_z on the surface roughness evaluation with ball end tooltips.

Hereafter, Fig. 14c presents the effect of the tool run-out. It is depicted that the effect of the lead angle on the lateral run-out is non-linear, with a bigger run-out at the center of the tool, increasing with the tool tilting, corroborating with the higher roughness found with a tilting increase (Table 3). It also can be seen that even run-out decreases with the tool height, it is still higher than the difference in magnitude of the measured tooth in the Zoller presetter (~15 μm), supporting the idea that only one tooth of the tool generates the final surface.

Lastly, the application of the proposed methodology is presented on a section of the machined blade, locally evaluating the spiral toolpath used in the manufacture. The results depicted in Fig. 15 allow the visualization of the very uneven CL points distribution (red dots) calculated by the CAM software. A significant number are located on surface regions with high curvature (small surface local radius),

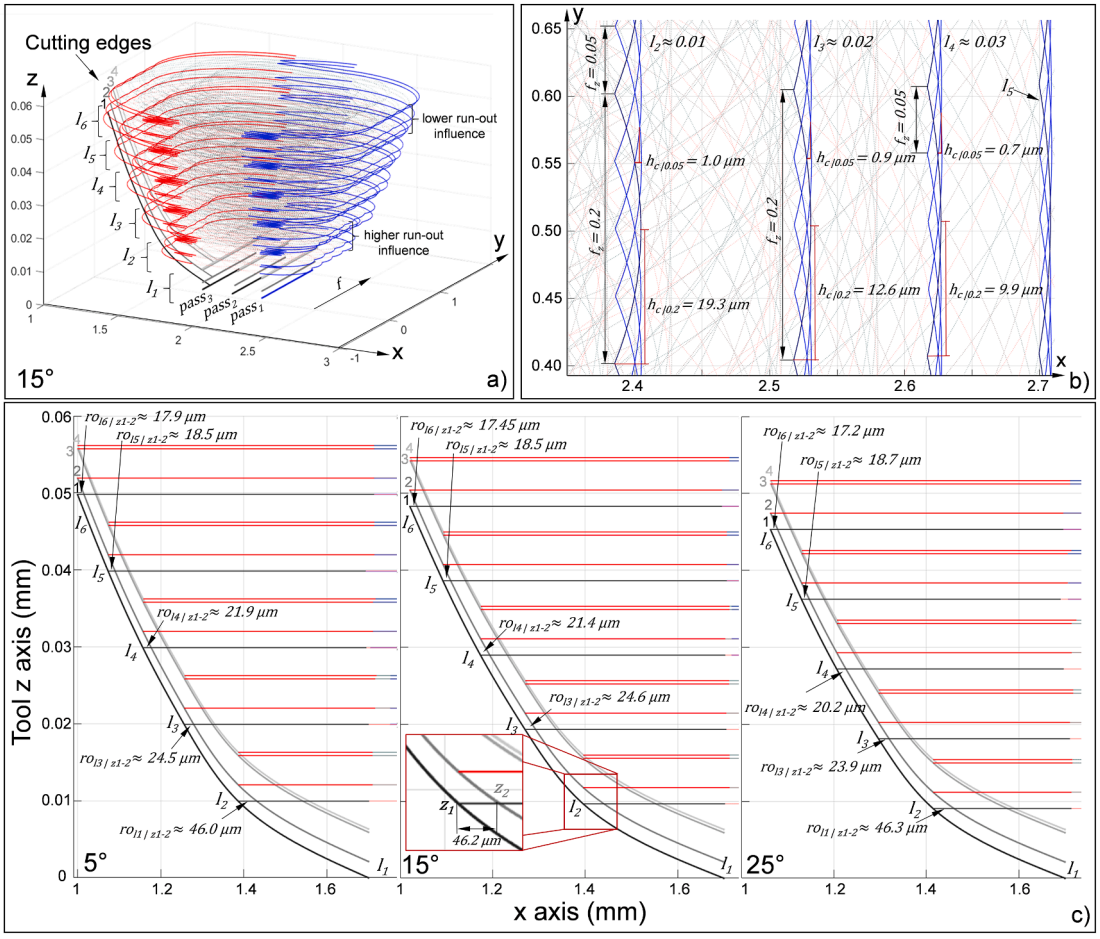

Fig. 14. a) Simulation of the ICE trochoidal movement: a) isometric view of 3 passes with 15° lead angle; b) top view and theoretical lateral roughness using two levels of *feed-per-tooth; c) lateral tool run-out on six tool heights considering 5, 15, and 25 lead angles.*

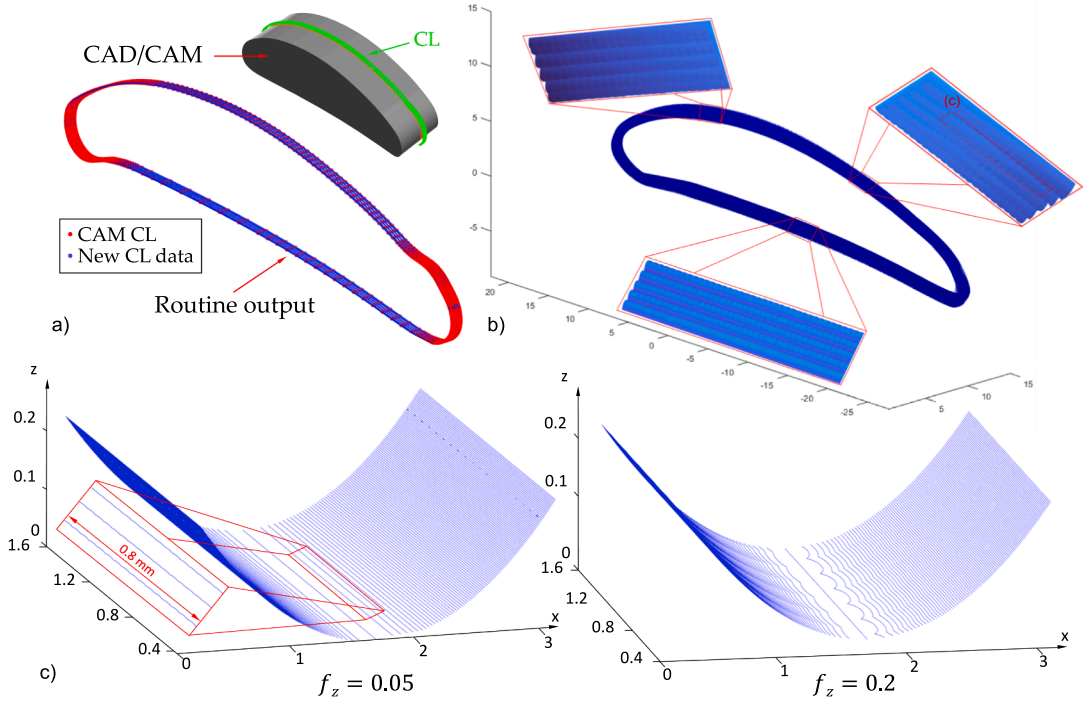

Fig. 15. a) CAM programming and refined data obtained by the routine for a blade profile; b) simulation of the surface using the treated data; c) ICE trochoidal movement on an infinitesimal plane.

indicating the necessity of data normalization for a proper prediction. Therefore, the developed routine facilitates the data output with a more even distribution and considers the feed-per-tooth marks of 5-axis profiles over the hole surface, as can be seen in Fig. 15b.

However, the data cloud generated and the complexity of generating the intersections or contours in highly curvy free-form surfaces limit the direct implementation of the trochoidal movement of the ICE element. Still, the developed model is a powerful tool that allows for obtaining texture aspects and the theoretical roughness of the machined surface locally by an infinitesimal approach, as presented in Fig. 15c.

4. Conclusions

In this work, it was observed that the CAM simulation does not provide a real estimation of the surface because it did not consider the crest height in the feed direction. Thus, the contact of the tool with the instantaneous surface was mathematically modeled to identify the final surface topography and the trochoidal movement of the instantaneous cutting-edge element along the toolpath. A routine for data acquisition using CAD/CAM software with an open interface was developed to support the modeling, providing information on the instantaneous positions of the tool and surface. The proposed routine and model were evaluated through roughness prediction on a blade of Ni-Cr-based alloy manufactured in 5-axis milling with different tool inclinations. The main conclusions are:

- The developed model allowed the simulation of the crest height in the direction of the lateral depth of cut (a_e) and on the feed direction (f), which the commercial CAM software does not compute, and also provides the identification of the number of the tooth that generates the final surface for a more accurate topography prediction.
- In the ball end milling with a lead angle of 5 degrees, even with the tooltip center not participating in the cut, its nearby region and low effective cutting speed affected the final surface, propitiating a plastic deformation dominance, making it hard to identify the characteristic cusp marks of the process, and propitiating a higher discrepancy to the simulated surface. In this specific case, the plowing modeling is still necessary for improved surface prediction. Nevertheless, this combination resulted in lower roughness due to a lack of crest heights.
- In cases of 15 and 25 lead angles due to the tool run-out, only an edge of the tool generates the final surface, a fact proved through the crest height modeling, run-out measuring, and confocal imaging analysis. The modeling process showed the capability of adjusting and improving the topography prediction with the input of the measured run-out and the calculated crest height.
- The developed routine propitiates a discretized output file for an arbitrary toolpath generated in a 5-axis CAM with automatic selection of the features involved, providing important data for modeling using both CL, CC with its respective vectors related to the tool and surface in a given instant.
- The evaluation of crest height showed that the lead angle affects the run-out and the effective cutting speed, influencing the surface texture. Also, the simulation of the movement of the ICE elements allowed the identification of the higher the element position in relation to the tool reference system, the lower the effect of the tool run-out.
- Even though the modeling results presented a good correlation between the feed marks and the measured topography, the errors associated with the theoretical crest height were still significant (about four times), and the effects of the effective cutting speed of the tooltip, feed rate oscillation, tool run-out, and cutting parameters which can be addressed in future works toward robust free-form surface modeling.

5. Future works

Even though it has been possible to quantify the local crest height marks with the free-form surface discretization, the proposed model cares for a graphical representation of the surface considering the movement of the ICE elements of the tooltip, which is the focus of future work.

Also, the proposed method can be expanded to simulate more complex problems of the free-form milling process, including the CWE and material properties information to compute the components of the cutting forces, permitting the estimation of tool deflection, geometric deviation, and tool wear, among others. Also, the model can be improved by addressing other factors, such as the instantaneous effective cutting speed and the feed rate oscillation during the milling process towards a robust surface texture modeling with ball-end tooltips.

CRediT authorship contribution statement

Felipe Marin: Data curation, Formal analysis, Investigation, Methodology, Software, Validation, Visualization, Writing – original draft, Writing – review & editing. **Adriano Fagali de Souza:** Conceptualization, Formal analysis, Investigation, Methodology, Supervision, Writing – review & editing. **Helton da Silva Gaspar:** Data curation, Formal analysis, Investigation, Methodology, Supervision, Visualization, Writing – review & editing. **Amaia Calleja-Ochoa:** Conceptualization, Project administration, Resources, Supervision, Validation, Visualization, Funding acquisition, Software. **Luis Norberto López de Lacalle:** Conceptualization, Methodology, Project administration, Resources, Supervision, Visualization.

Declaration of competing interest

The authors declare that they have no known competing financial interests or personal relationships that could have appeared to influence the work reported in this paper.

Acknowledgment

The authors thank the support of the National Council for Scientific and Technological Development (CNPq) and the Basque Government for funding Excellence University groups IT 1573-22 for funding this research. Machining experiments were performed under grant PDC2021-121792-I00 from MCIN/AEI/10.13039/501100011033 and by European Union by Next Generation EU/PRTR.

References

[1] B. Denkena, V. Böß, D. Nespor, A. Samp, Kinematic and stochastic surface topography of machined TiAl6V4-parts by means of ball nose end milling, Procedia Eng. 19 (2011) 81–87, https://doi.org/10.1016/j.proeng.2011.11.083.
[2] B. Wang, Z. Liu, Y. Cai, X. Luo, H. Ma, Q. Song, Z. Xiong, Advancements in material removal mechanism and surface integrity of high speed metal cutting: A review, Int. J. Mach. Tools Manuf. 166 (2021) 1–32, https://doi.org/10.1016/j.ijmachtools.2021.103744.
[3] M. Habibi, O. Tuysuz, Y. Altintas, Modification of tool orientation and position to compensate tool and part deflections in five-axis ball end milling operations, J. Manuf. Sci. Eng. Trans. ASME 141 (2019) 1–9, https://doi.org/10.1115/1.4042019.
[4] L.N. de Lacalle, A. Lamikiz, J.A. Sánchez, M.A. Salgado, Toolpath selection based on the minimum deflection cutting forces in the programming of complex surfaces milling, Int. J. Mach. Tools Manuf. 47 (2007) 388–400, https://doi.org/10.1016/j.ijmachtools.2006.03.010.
[5] W. Ma, G. He, L. Zhu, L. Guo, Tool deflection error compensation in five-axis ball-end milling of sculptured surface, Int. J. Adv. Manuf. Technol. 84 (2015) 1421–1430, https://doi.org/10.1007/s00170-015-7793-8.
[6] R.T. Coelho, A.F. de Souza, A.R. Roger, A.M.Y. Rigatti, A.A.de L. Ribeiro, Mechanistic approach to predict real machining time for milling free-form geometries applying high feed rate, Int. J. Adv. Manuf. Technol. 46 (2010) 1103–1111, https://doi.org/10.1007/s00170-009-2183-8.
[7] A.F. de Souza, R.B. Käsemodel, M. Arias, F. Marin, A.R. Rodrigues, Study of tool paths calculated by different commercial CAM systems and influences on the real machining time and surface roughness for milling free-form geometries,

J. Brazilian Soc. Mech. Sci. Eng. 41 (2019) 363, https://doi.org/10.1007/s40430-019-1865-x.
[8] J. Beňo, I. Maňková, P. Ižol, M. Vrabel', An approach to the evaluation of multivariate data during ball end milling free-form surface fragments, Measurement. 84 (2016) 7–20, https://doi.org/10.1016/j.measurement.2016.01.043.
[9] A. Mamedov, S.E. Layegh K, I. Lazoglu, Instantaneous tool deflection model for micro milling, Int. J. Adv. Manuf. Technol. 79 (2015) 769–777, https://doi.org/10.1007/s00170-015-6877-9.
[10] M. Aurrekoetxea, I. Llanos, O. Zelaieta, L.N. López de Lacalle, Towards advanced prediction and control of machining distortion: A comprehensive review, Int. J. Adv. Manuf. Technol. 122 (2022) 2823–2848, https://doi.org/10.1007/s00170-022-10087-5.
[11] B. Denkena, V. Böß, D. Nespor, P. Gilge, S. Hohenstein, J. Seume, Prediction of the 3D surface topography after ball end milling and its influence on aerodynamics, Procedia CIRP (2015) 221–227, https://doi.org/10.1016/j.procir.2015.03.049. Elsevier.
[12] I. Lazoglu, S.Y. Liang, Analytical modeling of force system in ball-end milling, Mach. Sci. Technol. 1 (1997) 219–234, https://doi.org/10.1080/10940349708945648.
[13] C. Zhang, S. Guo, H. Zhang, L. Zhou, Modeling and predicting for surface topography considering tool wear in milling process, Int. J. Adv. Manuf. Technol. 68 (2013) 2849–2860, https://doi.org/10.1007/s00170-013-4989-7.
[14] S.E. Layegh K, H. Erdim, I. Lazoglu, Offline force control and feedrate scheduling for complex free form surfaces in 5-axis milling, Procedia CIRP (2012) 96–101, https://doi.org/10.1016/j.procir.2012.04.015. Elsevier.
[15] E. Artetxe, G. Urbikain, A. Lamikiz, L.N. López-De-Lacalle, R. González, P. Rodal, A Mechanistic Cutting Force Model for New Barrel End Mills, in: Procedia Eng., No longer published by Elsevier, 2015: pp. 553–560. https://doi.org/10.1016/j.proeng.2015.12.532.
[16] S.E. Layegh K, I. Lazoglu, 3D surface topography analysis in 5-axis ball-end milling, CIRP Ann. – Manuf. Technol. 66 (2017) 133–136, https://doi.org/10.1016/j.cirp.2017.04.021.
[17] Q. Guo, W. Wang, Y. Jiang, Y. Sun, 3D surface topography prediction in the five-axis milling of plexiglas and metal using cutters with non-uniform helix and pitch angles combining runout, J. Mater. Process. Technol. 314 (2023) 117885, https://doi.org/10.1016/J.JMATPROTEC.2023.117885.
[18] Z.C. Wei, M.L. Guo, M.J. Wang, S.Q. Li, J. Wang, Prediction of cutting force for ball end mill in sculptured surface based on analytic model of CWE and ICCE, Mach. Sci. Technol. 23 (2019) 688–711, https://doi.org/10.1080/10910344.2019.1575408.
[19] L.N. López de Lacalle, A. Lamikiz, M.A. Salgado, S. Herranz, A. Rivero, Process planning for reliable high-speed machining of moulds, Int. J. Prod. Res. 40 (2002) 2789–2809, https://doi.org/10.1080/00207540210140068.
[20] J. Fei, F. Xu, B. Lin, T. Huang, State of the art in milling process of the flexible workpiece, Int. J. Adv. Manuf. Technol. 109 (2020) 1695–1725, https://doi.org/10.1007/S00170-020-05616-Z.
[21] W. Mou, S. Zhu, M. Zhu, L. Han, L. Jiang, A prediction model of cutting force about ball end milling for sculptured surface, Math. Probl. Eng. 2020 (2020), https://doi.org/10.1155/2020/1389718.
[22] B. Ozturk, I. Lazoglu, H. Erdim, Machining of free-form surfaces. Part II: Calibration and forces, Int. J. Mach. Tools Manuf. 46 (2006) 736–746, https://doi.org/10.1016/j.ijmachtools.2005.07.037.
[23] L.T. Tunc, E. Budak, Extraction of 5-axis milling conditions from CAM data for process simulation, Int. J. Adv. Manuf. Technol. 43 (2009) 538–550, https://doi.org/10.1007/s00170-008-1735-7.
[24] P. Muthuswamy, K. Shunmugesh, Artificial intelligence based tool condition monitoring for digital twins and industry 4.0 applications, Int. J. Interact. Des. Manuf. 17 (2022) 1067–1087, https://doi.org/10.1007/S12008-022-01050-5.
[25] J. Xu, L. Xu, Z. Geng, Y. Sun, K. Tang, 3D surface topography simulation and experiments for ball-end NC milling considering dynamic feedrate, CIRP J. Manuf. Sci. Technol. 31 (2020) 210–223, https://doi.org/10.1016/J.CIRPJ.2020.05.011.
[26] Y. Quinsat, L. Sabourin, C. Lartigue, Surface topography in ball end milling process: Description of a 3D surface roughness parameter, J. Mater. Process. Technol. 195 (2008) 135–143, https://doi.org/10.1016/j.jmatprotec.2007.04.129.
[27] R.A. Mali, T.V.K. Gupta, J. Ramkumar, A comprehensive review of free-form surface milling– Advances over a decade, J. Manuf. Process. 62 (2021) 132–167, https://doi.org/10.1016/J.JMAPRO.2020.12.014.
[28] I. Scandiffio, A.E. Diniz, A.F. de Souza, The influence of tool-surface contact on tool life and surface roughness when milling free-form geometries in hardened steel, Int. J. Adv. Manuf. Technol. 92 (2017) 615–626, https://doi.org/10.1007/s00170-017-0093-8.
[29] G. Urbikain, L.N.L. de Lacalle, Modelling of surface roughness in inclined milling operations with circle-segment end mills, Simul. Model. Pract. Theory 84 (2018) 161–176, https://doi.org/10.1016/j.simpat.2018.02.003.
[30] C. Nan, D. Liu, Analytical calculation of cutting forces in ball-end milling with inclination angle, J. Manuf. Mater. Process. 2 (2018) 35, https://doi.org/10.3390/JMMP2020035.
[31] I. Basso, R. Voigt, A.R. Rodrigues, F. Marin, A.F. de Souza, L.N.L. de Lacalle, Influences of the workpiece material and the tool-surface engagement (TSE) on surface finishing when ball-end milling, J. Manuf. Process. 75 (2022) 219–231, https://doi.org/10.1016/j.jmapro.2021.12.059.
[32] M.F. Batista, A.R. Rodrigues, R.T. Coelho, Modelling and characterization of roughness of moulds produced by high-speed machining with ball-nose end mill, Proc. Inst. Mech. Eng. Part B J. Eng. Manuf. 231 (2017) 933–944, https://doi.org/10.1177/0954405415584898.
[33] E.L. de Oliveira, A.F. de Souza, A.E. Diniz, Evaluating the influences of the cutting parameters on the surface roughness and form errors in 4-axis milling of thin-walled free-form parts of AISI H13 steel, J. Brazilian Soc. Mech. Sci. Eng. 40 (2018) 1–10, https://doi.org/10.1007/s40430-018-1250-1.
[34] J.S. Chen, Y.K. Huang, M.S. Chen, A study of the surface scallop generating mechanism in the ball-end milling process, Int. J. Mach. Tools Manuf. 45 (2005) 1077–1084, https://doi.org/10.1016/j.ijmachtools.2004.11.019.
[35] Q. Liu, J. Cheng, Y. Xiao, M. Chen, H. Yang, J. Wang, Effect of tool inclination on surface quality of KDP crystal processed by micro ball-end milling, Int. J. Adv. Manuf. Technol. 99 (2018) 2777–2788, https://doi.org/10.1007/s00170-018-2622-5.
[36] K. Groß, M. Eifler, K. Klauer, K. Huttenlochner, B. Kirsch, C. Ziegler, J.C. Aurich, J. Seewig, Determination of the surface topography of ball end micro milled material measures, Eng. Sci. Technol. Int. J. 24 (2021) 543–555, https://doi.org/10.1016/j.jestch.2020.08.005.
[37] E. Ozturk, L.T. Tunc, E. Budak, Investigation of lead and tilt angle effects in 5-axis ball-end milling processes, Int. J. Mach. Tools Manuf. 49 (2009) 1053–1062, https://doi.org/10.1016/j.ijmachtools.2009.07.013.
[38] X.-W. Liu, K. Cheng, A.P. Longstaff, M.H. Widiyarto, D. Ford, Improved dynamic cutting force model in ball-end milling. Part I: Theoretical modelling and experimental calibration, Int. J. Adv. Manuf. Technol. 26 (2005) 457–465, https://doi.org/10.1007/s00170-003-2014-2.
[39] Mitutoyo, Form Measurement Practical tips for laboratory and workshop, 2009. https://www.mitutoyo.com/webfoo/wp-content/uploads/Surface_Roughness_Measurement.pdf (accessed October 18, 2023).
[40] A.F. de Souza, E. Berkenbrock, A.E. Diniz, A.R. Rodrigues, Influences of the tool path strategy on the machining force when milling free form geometries with a ball-end cutting tool, J. Brazilian Soc. Mech. Sci. Eng. 37 (2015) 675–687, https://doi.org/10.1007/s40430-014-0200-9.